

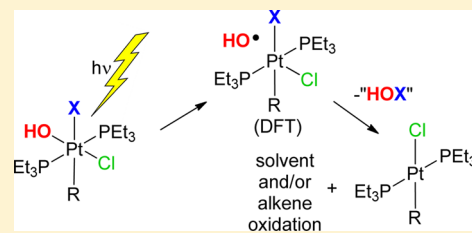
Photoreduction of Pt(IV) Halo-Hydroxo Complexes: Possible Hypohalous Acid Elimination

Lasantha A. Wickramasinghe and Paul R. Sharp*

Department of Chemistry, University of Missouri—Columbia, 125 Chemistry Building, Columbia, Missouri 65211-7600, United States

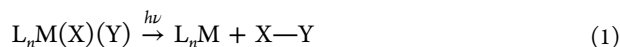
Supporting Information

ABSTRACT: Concentrated hydrogen peroxide addition to *trans*-Pt(PEt₃)₂Cl(R) [1 (R = 9-phenanthryl), 2 (R = 4-trifluoromethylphenyl)] yields hydroxo-hydroperoxo complexes *trans*-Pt(PEt₃)₂(Cl)(OOH)(OH)(R) [5 (R = 9-phenanthryl), 4 (R = 4-trifluoromethylphenyl)], where the hydroperoxo ligand is *trans* to R. Complex 5 is unstable and reacts with solvent CH₂Cl₂ to give *trans,cis*-Pt(PEt₃)₂(Cl)₂(OH)(9-phenanthryl) (3). Treatment of 4 with HCl yields analogous *trans,cis*-Pt(PEt₃)₂(Cl)₂(OH)(4-trifluoromethylphenyl) (6) and HBr gives *trans*-Pt(PEt₃)₂(Br)(Cl)(OH)(4-trifluoromethylphenyl) (7), where the Br and 4-trifluoromethylphenyl ligands are *trans*. Photolysis of 3 or 6 at 313 or 380 nm causes reduction to *trans*-Pt(PEt₃)₂Cl(R) (1 or 2, respectively). Expected coproduct HOCl is not detected, but authentic solutions of HOCl are shown to decompose under the reaction conditions. Chlorobenzene and other unidentified products that oxidize PPh₃ to OPPh₃ are detected in photolyzed benzene solutions. Photolysis of 3 or 6 in the presence of 2,3-dimethyl-2-butene (TME) yields the chlorohydrin (2-chloro-2,3-dimethyl-3-butanol), 3-chloro-2,3-dimethyl-1-butene, and acetone, all expected products from HOCl trapping, but additional oxidation products are also observed. Photolysis of mixed chloro-bromo complex 7 with TME yields the bromohydrin (2-bromo-2,3-dimethyl-3-butanol) and 2, consistent with *cis*-elimination of HOBr. Computational results (TDDFT and DFT) and photochemistry of related complexes suggest a dissociative triplet excited state reaction pathway and that HOCl elimination may occur by an incipient hydroxo radical abstraction of an adjacent halogen atom, but a pathway involving hydroxo radical reaction with solvent or TME to generate a carbon-based radical followed by halogen abstraction from Pt cannot be eliminated.



INTRODUCTION

Photoreductive elimination of an oxidant (XY) from a high oxidation state transition metal complex (eq 1) has been identified as an important step in potential solar energy conversion and storage.^{1,2} To be useful in such a scheme, these reactions should be endergonic and, as such, are plagued by the exergonic back reaction, reoxidation of the reduced transition metal complex, L_nM.



This problem may be able to be overcome by separation of the products into different phases.^{3,4} An alternative strategy is to follow the reductive elimination with conversion of the oxidant into a kinetically less reactive species. This could be the situation with hydrogen peroxide photoreductive elimination from a dihydroxo complex (eq 1, X = Y = OH) where the hydrogen peroxide decomposes into water and O₂.⁵ The O₂ is still a thermodynamically good oxidant, but it is kinetically less reactive than hydrogen peroxide and less likely to react with the reduced metal complex (L_nM).

There have been a few reports of hydrogen peroxide photoreductive elimination from dihydroxo complexes. Milstein⁵ reported apparent photoreductive elimination of hydrogen peroxide from a Ru dihydroxo complex, but only O₂ was detected, and computational studies⁶ dispute the intermediacy of hydrogen peroxide. More recently, the Pt(IV) dihydroxo complex *cis,trans,cis*-[PtCl₂(OH)₂(*cis*-1,4-DACH)] (DACH = diaminocyclohexane) was reported to photoeliminate H₂O₂

(detected by ¹H NMR).⁷ Thermal elimination was also reported suggesting a small free energy change for the reaction. Curiously, the H₂O₂ elimination is thought to occur from an oxo-bridged binuclear complex. Binuclear Tp*Cu(OH)₂CuTp* (Tp* = hydrotris(3,5-dimethyl-1-pyrazolyl)borate)⁸ and main group polyhydroxo complexes^{9,10} have also been reported to photoeliminate hydrogen peroxide.

We recently reported efficient molecular bromine photoelimination from the mononuclear Pt(IV) complexes *trans*-Pt(PEt₃)₂(R)-(Br)₃ (R = Br, aromatic carbonyl ligand).¹¹ These reactions suffer from back reaction of Br₂ with coproduct, *trans*-Pt(PEt₃)₂(R)(Br), and hence bromine traps must be added. With the idea of H₂O₂ instead of Br₂ photoelimination, we set out to prepare the analogous dihydroxo complexes *trans*-Pt(PEt₃)₂(R)(X)(OH)₂ (X = Cl, Br). Instead, we isolated monohydroxo complexes. While not the desired complexes, they are also highly photochemically active to net elimination, surprisingly of hypohalous acid (HOX, X = Cl, Br). Their synthesis and photochemistry is reported herein.

RESULTS

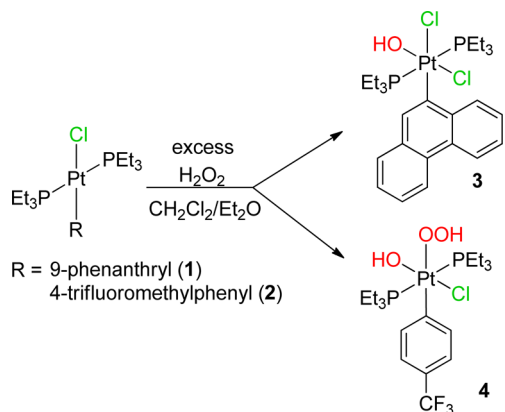
Complex Synthesis and Characterization. Pt(II) complexes *trans*-Pt(PEt₃)₂Cl(R) [1 (R = 9-phenanthryl), 2 (R = 4-trifluoromethylphenyl)] are resistant to oxidation by

Received: September 17, 2013

Published: January 21, 2014

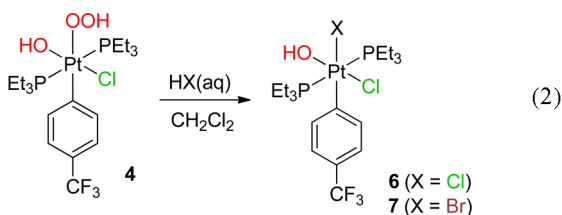
hydrogen peroxide and solutions (CH_2Cl_2 , THF, acetone) of the complexes remain unchanged when stirred with excess 30% aqueous hydrogen peroxide. However, slow oxidation does occur with concentrated diethyl ether solutions of hydrogen peroxide (Scheme 1). The reactions are accompanied by

Scheme 1



extensive decomposition of the hydrogen peroxide and can require multiple additions to complete. The final product depends on the R group. With R = 9-phenanthryl, the product is *trans,cis*-Pt(PEt_3)₂(Cl)₂(OH)(9-phenanthryl) (**3**). The source of the additional chloride is unknown, but because the isolated yield (68%) exceeds 50%, at least a portion of the chloride must originate from the CH_2Cl_2 solvent.

The reaction is more rapid with **2** than with **1**. However, the product is now the hydroxo-hydroperoxo complex *trans*-Pt(PEt_3)₂(Cl)(OH)(OOH)(4-trifluoromethylphenyl) (**4**). The NMR properties of **4** are similar to those of an intermediate (**5**) observed in the preparation of **3** and assigned as the 9-phenanthryl analogue of **4**. Complex **4** is readily converted to *trans,cis*-Pt(PEt_3)₂(Cl)₂(OH)(4-trifluoromethylphenyl) (**6**), an analogue of **3**, simply by the addition of aqueous HCl (eq 2, X = Cl). The same reaction with HBr(aq) yields the mixed bromo-chloro-hydroxo complex *trans*-Pt(PEt_3)₂(Br)(Cl)(OH)(4-trifluoromethylphenyl) (**7**).



Complexes **3**, **4**, **6**, and **7** gave crystals suitable for X-ray analysis. The solid-state structures of **3**, **4**, and **6** are shown in Figures 1, 2, and 3. Complex **7** is isomorphous and isostructural with **6** and also cocrystallized with ~20% **6** that was present as an impurity in the reaction mixture. Although the presence of a Br atom *trans* to the 4-trifluoromethylphenyl group is confirmed, the cocrystallization with **6** and disorder make the metrical parameters unreliable, and the structure of **7** will not be discussed. Selected metrical parameters for the other complexes are listed in Table 1 and have been averaged where chemically equivalent parameters are present.

Complexes **3** and **4** crystallized as hydrogen-bonded dimers. In the case of **3**, the dimer is asymmetric and only one of the

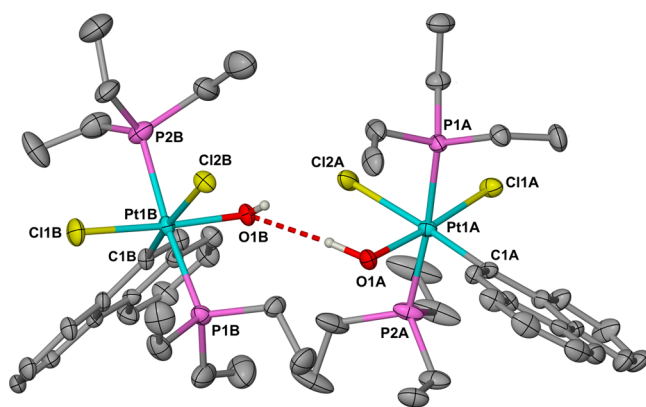


Figure 1. Solid-state structure of the hydrogen-bonded dimer of **3** (30% probability ellipsoids, hydrogen atoms omitted except for the OH-group hydrogen atoms, which are represented as arbitrary spheres).

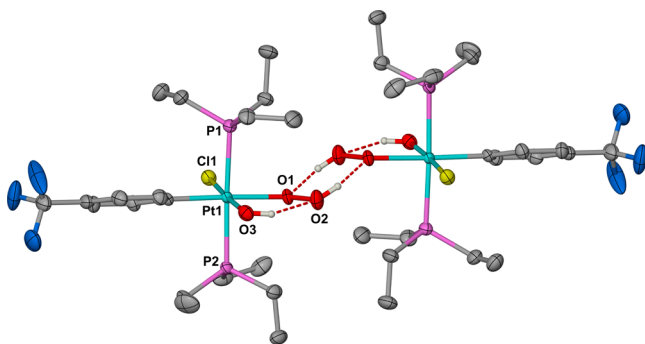


Figure 2. Solid-state structure of the centrosymmetric hydrogen-bonded dimer of **4** (50% probability ellipsoids, hydrogen atoms omitted except for the OH and OOH group hydrogen atoms, which are represented as arbitrary spheres).

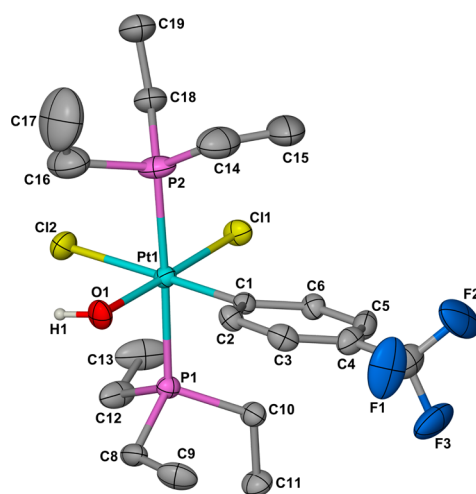


Figure 3. Solid-state structure of **6** (one of two independent molecules, 50% probability ellipsoids, hydrogen atoms omitted, except for the OH ligand hydrogen atom, which is represented as an arbitrary sphere). Rotational disorder in the CF_3 group is not shown.

hydroxo-group hydrogen atoms participates in the hydrogen bonding. In contrast, a centrosymmetric dimer is observed for **4**, and both the hydroxo and the hydroperoxo groups are involved in hydrogen bonding. However, only the hydroperoxo group participates in the intermolecular hydrogen bonding and

Table 1. Selected Mean^a Metrical Parameters for Chloro-Hydroxo Complexes **3** and **6** and Hydroperoxo-Hydroxo Complex **4**

	3	6	4
Pt–Cl1	2.356(6)	2.349(1)	2.3541(11) ^b
Pt–Cl2	2.444(2)	2.442(9)	
Pt–P	2.374(4)	2.371(6)	2.36(1)
Pt–OH	2.018(2)	2.028(5)	2.032(3) ^b
Pt–OOH			2.104(3) ^b
Pt–C	2.088(6)	2.050(1)	2.040(4) ^b
O–O			1.472(4) ^b
Cl1–Pt–Cl2	88.98(3)	92.0(6)	
Cl1–Pt–P	87.5(8)	90(1)	88.23(4) ^b (P1) 93.05(4) ^b (P2) mean = 91(3)
Cl2–Pt–P	87(1)	89(3)	
	89(1) ^c		
Cl1–Pt–OH	175(1)	178.2(6)	176.47(9) ^b
Cl1–Pt–OOH			84.98(9) ^b
Cl2–Pt–OH	86(1)	86(1)	
Cl1–Pt–C1	98(1)	93.3(1)	94.96(13) ^b
Cl2–Pt–C1	172(1)	174(1)	
P–Pt–P	174.7(4)	177.8(1)	177.51(4) ^b
P–Pt–OH	91(1)	90(2)	89(3)
P–Pt–OOH	85.4(5) ^c		92.11(9) ^b (P1) 85.87(9) ^b (P2)
P–Pt–C1	90.9(6)	90.8(6)	91(2)
	92.8(5) ^c		
HO–Pt–C1	86.5(4)	88.4(4)	88.54(15) ^b
HO–Pt–OOH			91.54(12) ^b
C1–Pt–OOH			178.14(14) ^b
Pt–O1–O2			110.4(2) ^b

^aMean of chemically equivalent parameters with standard deviation in parentheses. ^bSingle value with estimated error in parentheses. ^cP atom of PEt₃ ligand near phenanthryl *peri*-hydrogen atom.

forms a six-membered ring through head-to-tail dimerization of the OOH group. Meanwhile, the hydroxo group is intramolecularly hydrogen bonded to the β-O of the hydroperoxo group. A similar hydrogen bonding arrangement is found in the dimer structure of Tp*Pt(OOH)(CH₃)₂ (Tp* = hydrotris(3,5-dimethylpyrazolyl)borate).¹²

Metrical parameters for the complexes are much as expected with essentially identical Pt–P and Pt–Cl distances for all three complexes. The Pt–OH and Pt–C distances in the phenanthryl complex (**3**) differ slightly from those in the CF₃–phenyl complexes (**4** and **6**). The Pt–C distance is longer in **3**, possibly due to steric interactions of the *peri*-hydrogen atom of the phenanthryl group with the *cis*-PEt₃ and -Cl ligands, although electronic factors may also be involved. The steric effect of the *peri*-hydrogen atom is evident in the angles around the Pt center, which deviate more from the ideal 90° and 180° angles in **3** than in **6**. (For examples of *peri*-hydrogen steric interaction in Pt(IV) organometallic complexes, see ref 11.) Larger deviations are also seen in **4** and may be associated with the hydrogen bonding.

Complex **4** is preceded by two crystallographically characterized Pt(IV) η¹-hydroperoxo complexes: Pt(tmeda)-(OOH)(OCH₃)(CH₃)₂¹³ and Tp*Pt(OOH)(CH₃)₂ (Tp* = hydrotris(3,5-dimethylpyrazolyl)borate).¹² Crystallographic problems with the tmeda structure make the metrical

parameters unreliable. Comparison of the O–O bond distance and the Pt–O–OH angle in the Tp* complex to those in **4** shows that they are essentially identical; however, the Pt–OOH distances differ markedly being longer by ~0.1 Å in **4**. This is likely due to a difference in the donor *trans* to the OOH ligand. In **4**, it is a strong *trans*-influence aryl ligand, while in the Tp* complex it is a weaker *trans*-influence pyrazolyl group of the Tp* ligand.

The hydroxo complexes **3** and **6** are new members of a very small group of structurally characterized Pt(IV) hydroxo complexes containing a phosphine ligand. While there are many structurally characterized Pt(IV) hydroxo complexes with a variety of ligands,¹⁴ only *fac*-Pt(dppbz)Me₃(OH) (dppbz = *o*-bis(diphenylphosphino)-benzene)¹⁵ and [Pt(PCN)(OH)₂(H₂O)]BF₄ (PCN = C₆H₃[CH₂P(*t*-Bu)₂](CH₂)₂N(CH₃)₂)¹⁶ contain a phosphine ligand. Unfortunately, the hydroxo and aqua ligands were not differentiated in the PCN complex. In the dppbz complex, the OH group is *trans* to a strong *trans*-influence methyl group, and the Pt–OH distance, 2.116(7) Å, is consequently longer than the 2.018(2) and 2.028(5) Å distances observed in **3** and **6**.

The stereochemistry of the Pt centers in **3**, **4**, **6**, and **7** is established by the X-ray structures and places the phosphine ligands *trans* to each other and the hydroxo group *cis* to the R group. While less definitive, the NMR data for the complexes is consistent with the solid-state results. A single phosphine ³¹P NMR resonance with ¹⁹⁵Pt satellites is observed. The J_{PtP} values are typical of similar Pt(IV) complexes (1700–1800 Hz) with *trans*-PEt₃ ligands and, as expected, are reduced from the parent Pt(II) complexes **1** and **2**.¹¹ Separate signals are observed for the phenyl ring protons in the ¹H NMR spectra of **4**, **6**, and **7**. This signifies a nonrotating phenyl ring on the NMR time scale and an asymmetric environment for the aryl ligand. For **6**, this would only be consistent with the OH ligand and a Cl ligand being *cis* to the phenyl ring, as observed in the solid-state structure.

The complexes also show evidence of hydrogen bonding and exchange in their solution NMR spectra. ³¹P NMR chemical shifts for **3** are sensitive to the presence of H₂O such that there are slight differences in the shift (δ ~1) observed for the isolated complexes and those for the reaction mixtures that contain water from H₂O₂ decomposition. In addition, an OH signal (δ –0.13) is not observed in the ¹H NMR spectrum of **3** unless protic impurities are removed by treatment of the NMR sample with base. For **4**, **6**, and **7**, ¹H NMR spectra in CDCl₃ show peaks for the OH ligand at δ 0.20 (**4**), –0.48 (**6**), and –0.6 (**7**). The OOH ligand of **4** is found at δ 6.42. The OH and OOH signals are concentration dependent for **4** and **6**. (This is presumably also true of **7**, but this was not investigated.) With increasing concentration the signals broaden and the OH signals, which have ¹⁹⁵Pt satellites (40 Hz), begin to lose their coupling to the Pt center. In C₆D₆, the OH signal for **6** lacks satellites, even in dilute solutions, suggesting more rapid exchange than that in CDCl₃, probably resulting from a greater tendency to form hydrogen-bonded dimers.

The UV–vis absorption spectra for **3** and **6** are given in Figure 4. As expected from their pale yellow color, the spectra show only a tail-off from the UV into the visible. The spectrum of **3** is much more intense in the UV than that for **6** and is likely dominated by absorptions associated with the phenanthryl moiety. In particular, the vibronically coupled π–π* transitions are usually located in the 300 nm region, and the bands in this region in the spectrum of **3** can be thus assigned. In contrast, the higher energy aryl group π-system in **6** will shift such bands

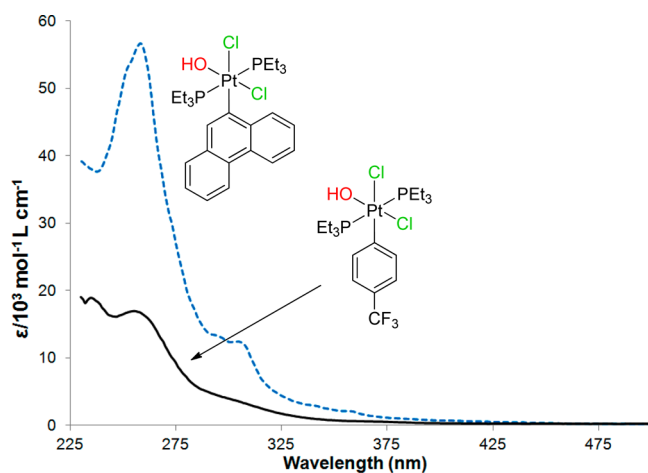


Figure 4. UV–visible absorption spectra of **3** and **6** in dichloromethane.

to higher energy exposing more Pt centered transitions. because we are more interested in the Pt centered transitions, we will focus on the spectrum of **6**.

To help in the assignment of the low-UV bands in **6**, a TDDFT (CAM-B3LYP, pcm) study was undertaken with model complex *trans,cis*-Pt(PMe₃)₂(Cl)₂(OH)(4-trifluoromethylphenyl), **6'**, where the PEt₃ ligands of **6** are replaced by PMe₃ ligands. The calculated vertical singlet transition energies and oscillator strengths (Table 2) over the region of the

Table 2. Vertical Singlet Transitions for **6'** in Dichloromethane^a

transition	wavelength	osc. strength	contributions (>3%)
1	365	0.0082	H – 3 → LUMO (56%) HOMO → LUMO (20%) H – 1 → LUMO (17%)
2	311	0.0054	H – 4 → LUMO (40%) H – 7 → LUMO (15%) HOMO → LUMO (12%) H – 5 → LUMO (8%)
3	304	0.0313	HOMO → LUMO (49%) H – 3 → LUMO (19%) H – 4 → LUMO (12%) HOMO → L + 1 (7%) H – 6 → LUMO (5%)
4	292	0.009	H – 1 → LUMO (65%) H – 3 → LUMO (13%) H – 1 → L + 1 (4%)

^aCAM-B3LYP, pcm.

experimental spectrum are displayed in Figure 5 along with the experimental spectrum. A good fit of the calculated transitions for **6'** to the experimental spectrum of **6** is observed, especially in the lower-energy region. The obtained orbital contributions to the transitions are fairly complex (Table 2 and Table S21, Supporting Information) and a natural transition orbital (NTO) analysis¹⁷ was applied for the five lowest-energy transitions. This yielded one dominant (eigenvalue ≥ 0.96) contributing orbital set for each transition. The NTO set for the first (lowest-energy) transition is graphically presented in Figure 6, and the remaining four are provided in the Supporting Information (Figures S36–S39). In common with the other

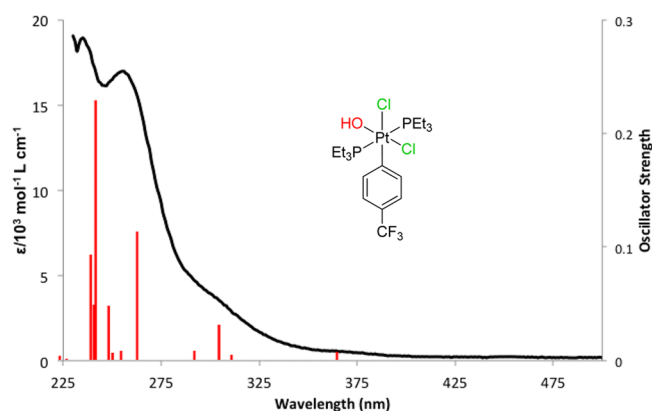


Figure 5. UV–visible absorption spectrum of **6** in dichloromethane with TDDFT (CAM-B3LYP, pcm) vertical transitions for **6'** (red vertical lines with the height corresponds to the oscillator strength).

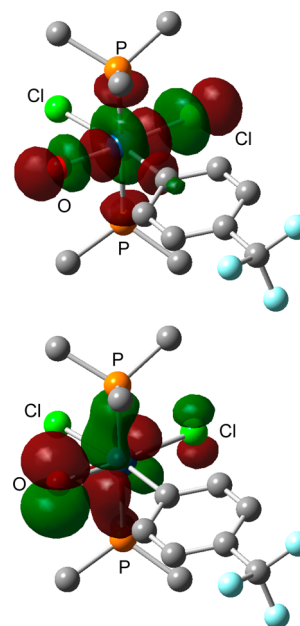
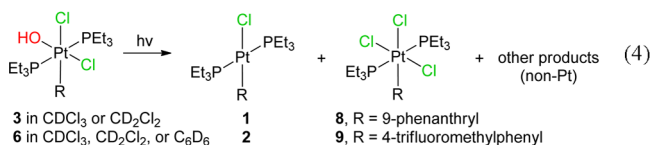
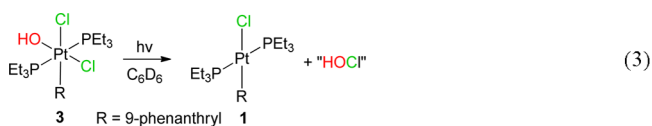


Figure 6. Natural transition orbital (NTO) set for the first singlet excited state of **6'** (isovalue = 0.04). The “arrival” orbital is on the top and the “departure” orbital is on the bottom (H atoms omitted).

four sets, the arrival orbital for the first transition is an e_g^* -type (pseudo-octahedral symmetry) orbital with strong antibonding interactions between the Pt and the OH and Cl ligands along the HO–Pt–Cl axis. The departure orbital is largely composed of an OH lone-pair and a matching t_{2g} -type Pt orbital, with minor P, C, and Cl components. The departure orbitals for the other three transitions are various combinations of Cl lone-pair, t_{2g} -type Pt, P, and π -aryl orbitals. The first five triplet excited-state transitions were also calculated (Table S22, Supporting Information), and the compositions and energies of the two lowest match closely to those of the corresponding singlets, suggesting facile singlet–triplet intersystem crossing at this level. Also possible is direct excitation into the triplet excited states at lower energies.

Photochemistry. Complexes **3** and **6** are photosensitive to light in the blue and UV regions. In C₆D₆ ($\lambda = 313$ nm), clean conversion of **3** to Pt(II) complex **1** is observed (eq 3) as indicated by ¹H and ³¹P NMR spectroscopy and by the observation of isosbestic points when the reaction is monitored

by UV–vis absorption spectroscopy (Figure S34, Supporting Information). Two Pt products are obtained for **6** in C_6D_6 and for both **3** and **6** in $CDCl_3$ and CD_2Cl_2 . The major products (60–80% yield) are again **1** and **2**, but significant amounts (10–35% yield) of the Pt(IV) complexes *trans,mer*-Pt(PEt_3)₂(Cl)₃R [R = 9-phenanthryl (**8**), R = 4-trifluoromethylphenyl (**9**)] are also obtained (eq 4).



By stoichiometry, the formation of **1** and **2** implies that **3** and **6** photoeliminate HOCl. To test for the possible presence of HOCl, PPh_3 was added to C_6D_6 solutions of **3** immediately after photoconversion (313 nm) to **1**. A 22% yield (based on **3**) of $OPPh_3$ (eq 5) was indicated by ^{31}P NMR spectroscopy. No

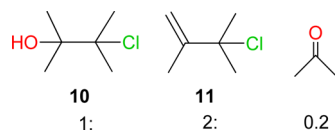


$OPPh_3$ is observed for the $CDCl_3$ and CD_2Cl_2 photoreaction mixtures. To help identify the oxidant in the photolyzed C_6D_6 solutions, 2,3-dimethyl-2-butene (TME) was added to a photolyzed solution of **3** in place of PPh_3 . The expected HOCl oxidation product, chlorohydrin **10**, is not observed, nor are other possible oxidation products (see below).

Because reaction conditions typically used to generate chlorohydrins from an alkene employ a large excess of HOCl in aqueous acid,¹⁸ very different from our potential reactions conditions of low HOCl concentration and nonprotic solvents, we studied HOCl reactions with TME under conditions similar to ours. Gaseous HOCl was generated by treating solid $Ca(OCl)_2$ with acid (H_2SO_4 or HCl)¹⁹ and was vacuum transferred into solution. Alternatively, HOCl solutions were prepared by the reaction of HgO and Cl_2 in water-saturated solvents.²⁰ HOCl formation was confirmed by UV–vis absorption spectroscopy after transfer to water (Figure S2, Supporting Information). Approximately 12 mol % ClO_2 was also detected in the HOCl from $Ca(OCl)_2$.

TME reactions with HOCl solutions were analyzed by 1H NMR spectroscopy and showed that chlorohydrin **10** is formed along with 3-chloro-2,3-dimethyl-1-butene (**11**) and acetone in about a 1:2:0.2 ratio (Chart 1). Thus, the oxidant in the

Chart 1. TME–HOCl Reaction Products^a



^aHOCl from H_2SO_4 and $Ca(OCl)_2$.

photolyzed solutions of **3** and **6** (eq 5) is not HOCl but probably a solvent-derived species. Attempts to detect 1H NMR signals for this species in photolyzed C_6H_6 solutions were not

successful, although chlorobenzene was detected in 50% yield (relative to **2**). Photolysis of HOCl solutions in C_6H_6 also produced chlorobenzene.

The absence of HOCl in photolyzed solutions of **3** and **6** is consistent with the low stability of HOCl in the presence of Pt complexes and under photolysis.²¹ Fresh benzene solutions of HOCl start out a characteristic yellow color but become colorless within 15 min and lose their ability to oxidize TME. Dichloromethane and chloroform solutions appear to be more stable (hours) but quickly decolorize under irradiation (313 or 380 nm), and the resulting solutions do not oxidize PPh_3 . Addition of *trans*-Pt(PEt_3)₂Cl(4-trifluoromethylphenyl) (**2**) to a fresh benzene solution of HOCl results in the immediate formation of trichloro Pt(IV) complex indicating that HOCl has been consumed. Thus, HOCl photoelimination from **3** and **6** may occur, but the HOCl would not survive the reaction conditions.

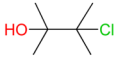
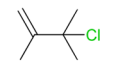
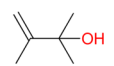
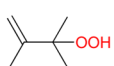
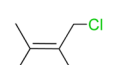
To further investigate the role of **2** in the possible decomposition of photoeliminated HOCl, the photolysis of **6** in the presence of an equimolar amount of **2** was examined. Photolysis proceeds as without added **2** (similar time scale), but the yield (based on **6**) of trichloro Pt(IV) complex **9** increases to 48%. From the amount of chlorine in **6**, the maximum possible yield of **9** is 50%. If this represents trapping of photoeliminated HOCl by **2**, the capture efficiency is 96%.

TME was added to photolysis solutions of **3** and **6** to serve as an HOCl trap. Photolysis proceeds as without added trap, but now the amount of **8** and **9** formed in $CDCl_3$ and CD_2Cl_2 is reduced to just traces. TME oxidation is observed and products from the CD_2Cl_2 and C_6D_6 reactions are listed in Tables 3 (**3**) and 4 (**6**). In common with HOCl, **11** and acetone are observed for **3**, but only small amounts of chlorohydrin (**10**) are detected, and several new products (**12**–**14**) are formed. Another product, formed in low yield, has a single 1H NMR signal and could be triacetone triperoxide,²² but this was not confirmed. In contrast to **3**, photolysis of **6** with TME in $CDCl_3$ and CD_2Cl_2 produces chlorohydrin **10** as a major product in addition to **11**, **12**, **14**, and acetone. Chlorohydrin **10** is the only detected TME product for **6** in C_6D_6 , but the yield is only 5%.

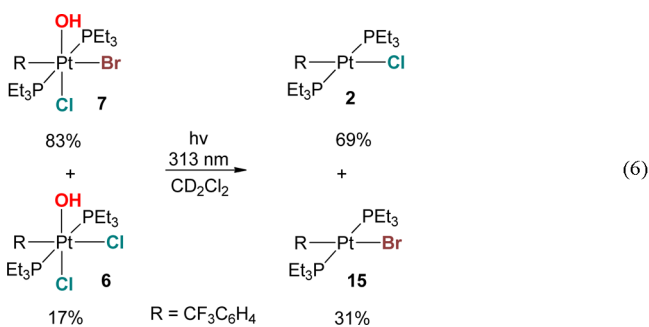
Hydroperoxide **13** is reported to be the major product of the TME reaction with singlet oxygen.²³ Its formation in the photolysis of **3** (Table 3) suggests triplet sensitization of O_2 with formation of singlet oxygen.²⁴ To investigate this possibility, the photolysis of **3** and TME was conducted in O_2 -saturated C_6D_6 solutions. (All other photolyses were conducted in vacuum-degassed solutions backfilled with Ar.) The yield of **13** increased greatly such that the total yield of oxygen-containing products exceeds that possible from **3** alone, clearly indicating the involvement of the added O_2 in product formation. Photolysis of an O_2 -saturated TME C_6D_6 solution does not produce **13**. Thus, if **13** is produced from singlet oxygen in the degassed solutions of **3**, the source of the O_2 must be **3**, possibly from decomposition of photoeliminated HOCl into O_2 and HCl . Photolysis of **6** with TME in O_2 -free and O_2 -saturated solutions (Table 4) does not produce **13**, indicating a difference in the photochemistry of **3** and **6**.

Complex **7** is also photochemically active. Photolysis of a mixture of **6** (17%) and **7** (83%) gives predominately **2** (69%) with lesser amounts of *trans*-Pt(PEt_3)₂(Br)(4-trifluoromethylphenyl) **15** (31%), both in the presence and in the absence of TME (eq 6). Seventeen percent of the yield of **2** is from **6** with the remaining 52% coming from **7**. Thus, the photolysis of **7**

Table 3. TME (0.1 M) Product Yields^a from Photolysis of 3 (10 mM)

TME Products	CD ₂ Cl ₂		C ₆ D ₆			
	(% yield) ^a		(% yield) ^a			
	380 nm ^b	313 nm	380 nm ^b	380 nm, ^b O ₂ saturated	313 nm	313 nm, ^b O ₂ saturated
 10	<1	7	2	2	0	2
 11	7	8	5	12	10	9
 12	4	5	<1	<1	5	<1
 13	20	10	21	65	26	90
 14	4	5	2	<1	<1	<1
Acetone	9	7	0	0	0	0
O atom yield ^c	45	34	24	133	57	183
Cl atom yield ^c	12	20	9	14	10	11

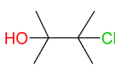
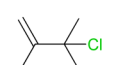
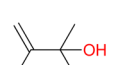
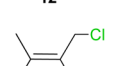
^aYields are relative to the molar amount of 2 with an estimated error of 1%. ^bShort (<6 min) high-intensity irradiations. ^cO atom yield = 10 yield + 12 yield + 2(13 yield) + acetone yield; Cl atom yield = 10 yield + 11 yield + 14 yield.



produces 2 and 15 in a 1:0.6 ratio suggesting that the reaction is primarily a net *cis*-photoelimination of the Br and OH groups. Consistent with HOBr photoelimination, TME products are primarily (21%) bromohydrin 16 (Chart 2) with no detectable chlorohydrin 10.

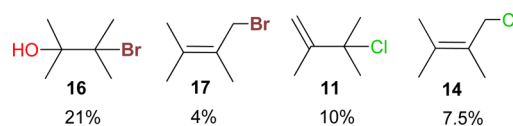
Computational Modeling. Previously, we found that the M06 functional gave gas-phase thermodynamic estimates for Br₂ oxidative addition to *trans*-PtL₂Br(R) complexes that matched well with toluene solution experimental measurements.¹¹ Extending these calculations to the current system using PMe₃ model complexes gave the free energies for reductive elimination of HOCl and Cl₂ in Scheme 2 (L = PMe₃). An estimate of the reductive elimination/oxidative addition barrier would be useful. However, to computationally determine the barrier, the mechanism must be known, and with the many possibilities, such a computational study is beyond the scope of this manuscript. We did try to induce

Table 4. TME Product Yields^a from Photolysis of 6 (18 mM, 313 nm)

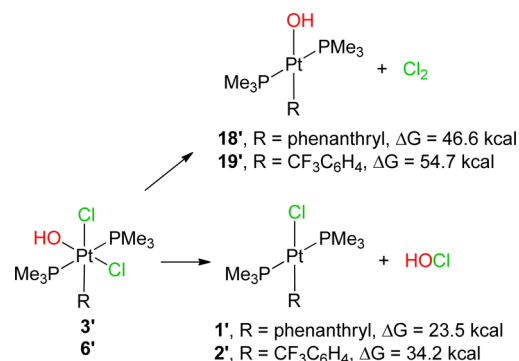
TME Products	CDCl ₃		CD ₂ Cl ₂	
	[TME]		[TME]	
	0.13 M	1.8 M	0.21 M, O ₂ saturated ^c	0.44 M
 10	18 %	26 %	13%	28 %
 11	7 %	9 %	5%	11 %
 12	3 %	23 % ^b	5%	7 %
 14	8 %	25 %	7%	18 %
Acetone	<1 %	5 %	10%	4 %
O atom yield ^d	22	54	31	39
Cl atom yield ^d	33	60	25	57

^aYields are relative to the molar amount of 2 with an estimated error of 1%. ^bTME impurities at this high concentration are significant and may interfere. ^c13 mM 6 (3% epoxide also formed). ^dO atom yield = 10 yield + 12 yield + acetone yield; Cl atom yield = 10 yield + 11 yield + 14 yield.

Chart 2



Scheme 2. DFT Gas-Phase Reductive Elimination Free Energies (25 °C, 1 atm)



reductive elimination by a stepwise reduction of the OH–Cl distance in 6', but no conversion was observed and the potential energy steadily increased by over 100 kcal/mol. We also looked for HOCl adducts of the Pt(II) complexes but found only very weak interactions (1–3 kcal/mol).

As expected, the reductive-elimination free energies for HOCl and Cl₂ from *trans,cis*-Pt(PMe₃)₂(Cl)₂(OH)(9-phenanthryl) (3')

and *trans,cis*-Pt(PMe₃)₂(Cl)₂(OH)(4-trifluoromethylphenyl) (**6'**) are positive, indicating thermodynamically unfavorable reactions but favorable reverse oxidative-addition reactions. Chlorine elimination is disfavored over HOCl elimination by ~20 kcal. The Cl–Cl bond enthalpy is ~2 kcal/mol greater than the HO–Cl bond enthalpy, slightly favoring Cl₂ elimination.²⁵ A Pt–OH bond that is significantly weaker than the Pt–Cl bond must be invoked to explain the favored HOCl elimination. Indeed, the calculated (M06) gas-phase bond dissociation enthalpies for **3'** and **6'** are 63.6 and 55.6 kcal/mol for the Pt–OH bond and 78.9 and 69.8 for the Pt–Cl bond. Thus, the Pt–Cl bond (*trans* to OH) in **3'** and **6'** is stronger than the Pt–OH bond by 14–15 kcal/mol.

The relaxed triplet structures for the Pt(IV) complexes were also explored. Two triplet structures (**3'^{T1}** and **3'^{T2}**) from **3'** and one (**6'^{T2}**) from **6'** were located at 40–45 kcal above the singlets in the gas phase. Inclusion of dichloromethane solvent (pcm, gas phase structures) in the calculation did not significantly alter the energy difference (by 2 kcal/mol for **6'^{T2}**). Drawings of **3'^{T1}** and **3'^{T2}** are given in Figure 7. That for **6'^{T2}** is

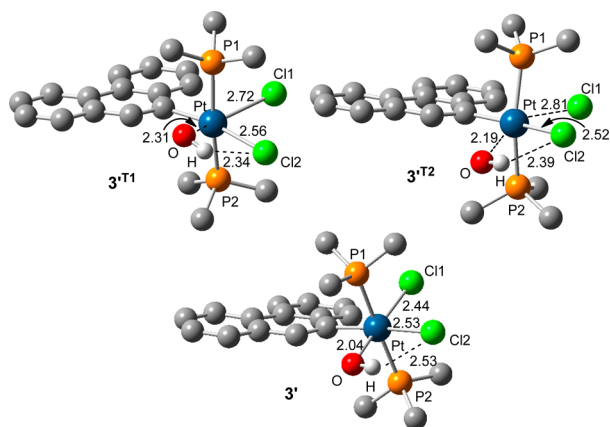


Figure 7. Triplet **3'^{T1}** and **3'^{T2}** and singlet **3'** structures (distances in Å, carbon-bonded H atoms omitted for clarity).

given in the Supporting Information (Figure S35). The structures **3'^{T2}** and **6'^{T2}** are similar and only **3'^{T1}** and **3'^{T2}** will be discussed. Triplets **3'^{T1}** and **3'^{T2}** have distorted octahedral geometries resulting from single occupancy of an e_g-type orbital. The two structures differ primarily in the extent of OH and Cl dissociation along the HO–Pt–Cl1 axis in the distorted octahedron. Both the Pt–OH and Pt–Cl1 distance increase by ca. 0.3 Å on going from **3'** to **3'^{T1}**. These distances also increase in **3'^{T2}** but the increase is dominated by the Pt–Cl1 distance, which increases by nearly 0.4 Å. Accompanying the Pt–Cl1 distance increase is a bending of the PMe₃ ligands in the direction of Cl1 such that the P1–Pt–P2 angle decreases from near linearity in **3'** to 159.6° in **6'^{T2}**. Changes in the Pt–C and Pt–Cl2 distances are less than 0.1 Å. Both triplets appear to have weak hydrogen bonding between the OH group and Cl2.

Dissociative triplet excited states are a common feature of d⁶-octahedral metal complexes and can result in ligand dissociation reactions, either with heterolytic or homolytic bond cleavage.^{26–32} The loss of an OH and a Cl radical from the triplets was examined by optimizing the Pt(III) doublets Pt(PMe₃)₂(Cl)₂(R) (**20'**, R = 9-phenanthryl; **21'**, R = 4-trifluoromethylphenyl) and Pt(PMe₃)₂(Cl)(OH)(R) (**22'**, R = 9-phenanthryl; **23'**, R = 4-trifluoromethylphenyl) derived from OH or Cl1 removal from

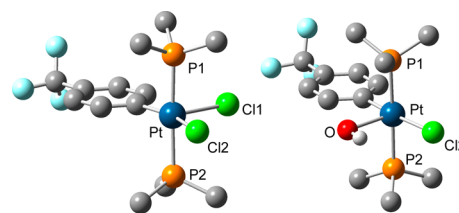


Figure 8. Doublet structures **21'** and **23'** (carbon-bonded H atoms omitted for clarity).

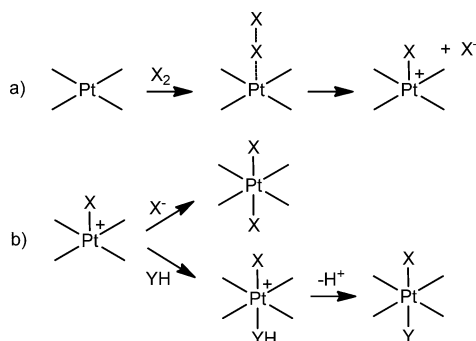
3' and **6'**. The resulting structures for R = 4-trifluoromethylphenyl are displayed in Figure 8. The optimized structures retain the parent configuration and are square pyramidal with a chloro or an hydroxo ligand in the axial position, although facile isomerization is expected for a square-pyramidal complex. Atomic spin density values (Table S20, Supporting Information) reveal spin density on the axial OH (0.3 e[−]) and Cl (0.5 e[−]) ligands suggesting substantial radical character for these ligands. (This is consistent with the first excited state NTO set in Figure 6.) Energetically, the loss of an OH group from either triplet, **3'^{T1}** or **3'^{T2}**, is nearly energetically neutral, while that from **6'^{T2}** is slightly (6 kcal) endergonic. Loss of a Cl atom from the triplets is unfavorable being ~18 kcal endergonic for **3'^{T1}** or **3'^{T2}** and 22 kcal endergonic for **6'^{T2}**.

Heterolytic bond cleavage with chloride and hydroxide ion dissociation was examined by optimization of the cations [Pt(PMe₃)₂(Cl)(OH)(4-trifluoromethylphenyl)]⁺ (**24'**) and [Pt(PMe₃)₂(Cl)₂(4-trifluoromethylphenyl)]⁺ (**25'**), derived from Cl1[−] and OH[−] removal from **6'**. The gas-phase free energies to dissociate an OH[−] from **6'** to give **24'** and a Cl[−] to give **25'** are, of course, very high (>100 kcal) due to charge separation without solvation. Applying a dichloromethane solvent correction (pcm model) lowers the free energies to 90.2 (**24'**) and 24.2 (**25'**) kcal. Relative to triplet **6'^{T2}**, the energies are 46.5 and −19.5 kcal. Clearly, hydroxide ion dissociation to **24'** is not favorable and unlikely to occur in this system. On the other hand, chloride ion dissociation appears favorable, at least in dichloromethane. However, with benzene as the solvent, an unfavorable energy of 60.4 kcal relative to **6'** (15.9 kcal relative to **6'^{T2}**) is obtained, indicating that even chloride ion dissociation is probably unfavorable in benzene.

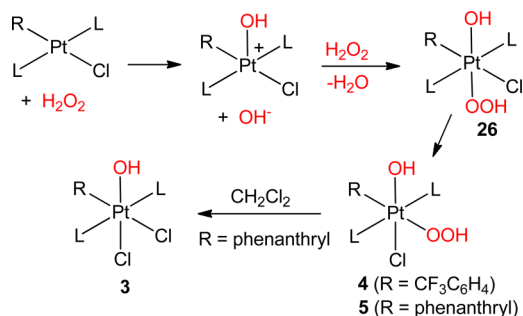
DISCUSSION

Syntheses. Pt(IV)-hydroxo complexes have been previously prepared by oxidative addition of H₂O₂ to Pt(II) complexes.^{33–39} However, this has been mostly restricted to Pt(II) complexes with amine or diimine ligands, research driven largely by the antitumor activity of Pt amine complexes. These reactions generally occur at, or slightly above, room temperature with 30% aqueous H₂O₂ to give dihydroxo complexes. The resistance of **1** and **2** to oxidation by 30% H₂O₂ was therefore unexpected but could be overcome with higher H₂O₂ concentrations. The Pt(II) oxidative addition mechanism for H₂O₂ has been proposed to be a three-centered concerted process⁴⁰ similar to C–H oxidative addition or to follow an ionic process similar to that for halogen oxidative addition: (a) oxidant electrophilic attack at an axial position with heterolytic cleavage of the oxidant and then (b) capture of the five-coordinate Pt(IV) cation by the oxidant anion or another available anion or ligand (Scheme 3).^{13,38,41} The capturing anion or ligand may also participate in the oxidation step by interaction with the Pt center opposite to the attacking oxidant, thereby bypassing the five-coordinate Pt(IV)

Scheme 3



Scheme 4



cation. In addition, isomerization can occur such that the final product does not contain a *trans* disposition of the added ligands.

Applying the ionic mechanism to the current system gives the proposed pathway to **3** and **4** given in Scheme 4. Here, capture of the five-coordinate cation (or assistance in the oxidation) is by high-concentration H_2O_2 , giving first *trans*-hydroperoxyhydroxo **26**, which then isomerizes to **4** or **5**. Complex **5** is unstable, possibly due to the strong labilizing effect of the *trans*-9-phenanthryl group, and reaction of the hydroperoxy ligand with CH_2Cl_2 yields chloride ion for formation of **3**. A relatively strong basic character for the hydroperoxy group is indicated by its selective protonation over the hydroxy group in the synthesis of **6** and **7** from **4** (eq 3).

Photochemistry. Understanding the photoreduction of **3** and **6** is challenging. Stoichiometry indicates HOCl elimination, but without direct detection of HOCl, other possibilities exist that could give the final stoichiometry without HOCl ever being formed. (A previous report of HOCl photoelimination from prolonged irradiation of Pt(IV) complexes assumes HOCl elimination by stoichiometry and bleaching of a dye.⁴²) Unfortunately, HOCl is not stable in the presence of Pt(II) complexes **1** and **2**, making direct detection difficult. Clearly, a strong oxidant is photochemically produced that oxidizes solvent benzene to chlorobenzene and other unidentified products that retain some oxidizing power and oxidize added PPh_3 . This behavior parallels that of a benzene solution of HOCl, which decomposes rapidly under photolysis (313 nm) and, just like in the photolysis of **3** and **6**, produces chlorobenzene and a solution that oxidizes PPh_3 .

Further support for HOCl formation is provided by the trapping experiments with **2** and TME. Complex **2** reacts with HOCl to produce trichloro complex **9**. Any HOCl produced in the photolysis of **6** could react with photogenerated **2** to produce **9**. In fact, **9** is observed in a 35% yield in the absence of added TME. Adding **2** at the beginning of the reaction increases the yield of **9** such that 96% of the theoretical HOCl

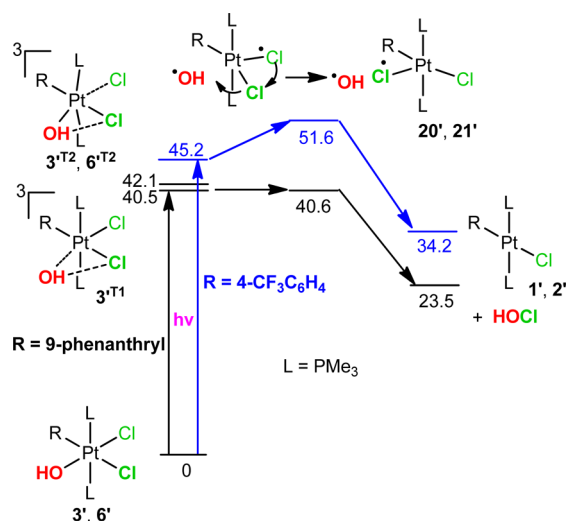
would have been consumed in the formation of **9** from **2**. With added TME, only traces of **9** form and the expected TME HOCl reaction products, chlorohydrin **10** and chlorinated **11**, are observed. However, the yield is rather low, especially for **3**, and a number of other products (**12–14**) are also produced, but these could arise from HOCl decomposition products.

Alternatives to HOCl elimination to consider are ionic and radical processes. Bromide photodissociation is reported for $[\text{PtBr}_6]^{2-}$ in water and MeOH,^{31,32,43–45} and we have shown that net bromide photodissociation also occurs in CH_2Cl_2 .¹¹ Chloride or hydroxide photodissociation from **3** or **6** would produce a Pt(IV) complex,⁴⁶ perhaps in an excited state and capable of alkene or even benzene oxidation. Alkene chlorination by Pd(IV) chloro complexes has been reported, and Pt(IV) complexes are involved in hydrocarbon oxidation in Shilov-type chemistry.^{47–50} Arguing against an ionic pathway is the absence of any significant change in reactivity and products on going from CH_2Cl_2 to benzene (at least for **3**) where ion formation should be disfavored. The DFT modeling of chloride and hydroxide photodissociation suggests that chloride dissociation is possible in CH_2Cl_2 , though probably not in benzene. Hydroxide dissociation is, however, unlikely.

Another ionic pathway to consider is excited-state, single-electron transfer (SET). This has been proposed for photoplatination of aromatic compounds with $[\text{PtCl}_6]^{2-}$ ⁵¹ and for $[\text{PtBr}_6]^{2-}$ photoreduction in the presence of high bromide ion concentrations⁵² or in methanol solution.⁵³ However, it was recently concluded that SET follows Br^- photodissociation for $[\text{PtBr}_6]^{2-}$.³² The photoreduction of **3**, **6**, and **7** proceeds equally well in the presence of electron-rich TME or simply in toluene, benzene, CH_2Cl_2 , or CDCl_3 solvent. Oxidation by SET in these various solvents seems unlikely.

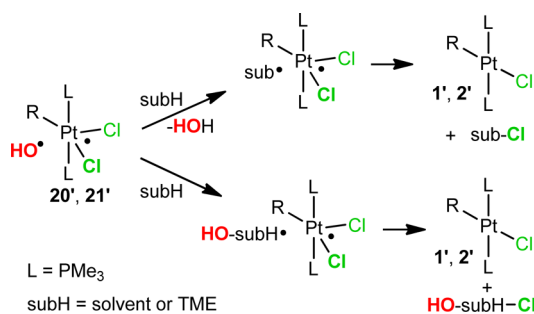
A radical reaction pathway would be consistent with the near solvent independence of the photochemistry of **3**, **6**, and **7**, and radical photoelimination from Pt(IV) is known. $[\text{PtCl}_6]^{2-}$ is thought to photoeliminate a chlorine atom,^{32,54–57} and Pt(IV) methyl complexes photoeliminate a methyl radical.⁵⁸ In addition, the DFT calculations on triplets $3'^{\text{T1}}$, $3'^{\text{T2}}$, and $6'^{\text{T2}}$ show large spin density on the OH and Cl axial ligands and elongation of the Pt–OH and Pt–Cl bonds, suggesting insipient formation of a geminate Pt(III)/OH radical pair from the triplet excited state. An OH or Cl radical would certainly be reactive enough to drive the photochemistry under a variety of conditions. According to the DFT calculations, OH radical formation is more favorable and the resulting Pt(III) complexes (modeled with **20'** and **21'**) have large spin densities on the axial Cl atoms, suggesting possible Cl atom abstraction from Pt by the OH radical (probably within the solvent cage) with net HOCl elimination. Dissociation of a Cl atom from the Pt(III) doublet complexes **20'** and **21'** is endergonic (32.6 and 33.3 kcal/mol, respectively) in the gas phase. Solvent inclusion (pcm, dichloromethane) gave only minor changes (<3 kcal/mol) in the dissociation energies. (Teets and Nocera suggested something similar for molecular halogen photoelimination from Au(III) halide complexes.⁴) To account for the preferred *cis*-elimination indicated by the photochemistry of bromo-hydroxy complex **7**, we propose that geometric isomerization of the five-coordinate Pt(II) complexes (**20'** and **21'**) interconverts the axial and equatorial chloro ligands bringing the former *cis*-chloro ligand into the axial position for abstraction by the OH radical. This pathway is summarized in Scheme 5 and assumes either direct excitation into the triplet manifold or rapid intersystem crossing following singlet excitation. TDDFT does indicate matching triplet

Scheme 5. Possible Photoelimination Pathway with DFT Gas-Phase Free Energies in kcal/mol for Model Complexes^a



^aBlack for R = 9-phenanthryl, blue for R = 4-CF₃C₆H₄.

Scheme 6. Substrate-Assisted *cis*-Elimination Pathway from Hydroxo Radical/Pt(III) Geminate Pair



transitions for the first two singlet transitions and small energy gaps, consistent with facile intersystem crossing.

An alternative to HOX elimination that could also follow from OH radical formation is depicted in Scheme 6. In this scheme, the OH radical either abstracts a hydrogen atom from solvent or TME or adds to solvent or TME. In either case, a carbon-based radical is then generated, which can abstract a halogen atom from the Pt(III) center. This scheme accounts for solvent oxidation, TME chlorination, and formation of the chlorohydrin.

CONCLUSIONS

The low kinetic reactivity of the Pt(II) phosphine complexes with H₂O₂ bodes well for H₂O₂ photoelimination from Pt(IV) dihydroxo complexes because this is the back reaction and H₂O₂ disproportionation may not be required to prevent it. When oxidation of the Pt(II) center by H₂O₂ does occur, the required high H₂O₂ concentrations result in trapping of the initial oxidation product with H₂O₂ and hydroperoxo-hydroxo complexes result instead of the expected dihydroxo complexes. Selective replacement of the hydroperoxo ligand with a halide ligand can occur spontaneously in CH₂Cl₂ or by treatment with HX.

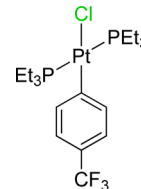
The photochemistry of the hydroxo-halo complexes is net HOX elimination. The photochemical pathway most consistent with the behavior of the system (trapping products and solvent insensitivity) and the DFT modeling is excitation into the lowest energy triplet excited state (either directly or via internal

conversion and intersystem crossing) followed by geminate Pt(III)/hydroxo radical pair formation. The hydroxo radical can then either abstract a halogen atom from the Pt(III) center forming HOX that decomposes and reacts with solvent or trap or react directly with the alkene trap or solvent to produce a carbon-based radical that then abstracts a halogen from the Pt(III) center. Both processes could be operating simultaneously.

EXPERIMENTAL SECTION

General Considerations. Pt(PET₃)₄⁵⁹ was prepared by a reported procedure. Reagents and solvents were purchased from commercial sources (Aldrich or Acros). Synthetic procedures were performed without exclusion of air with unpurified solvents unless otherwise noted. Platinum complex photolysis samples were prepared under a dinitrogen atmosphere in a Vacuum Atmospheres Corporation drybox or on a Schlenk line. Photolysis solvents were dried, degassed, and stored under dinitrogen over 4 Å molecular sieves. NMR spectra were recorded on Bruker AMX-250, -300, or -500 spectrometers at ambient probe temperatures except as noted. NMR shifts are given in δ with positive values downfield of tetramethylsilane, Si(CH₃)₄ (¹H and ¹³C), external H₃PO₄ (³¹P), external CFCl₃ (¹⁹F), or external K₂PtCl₄ (aq) (¹⁹⁵Pt, δ -1630). ¹³C, ¹⁹F, ¹⁹⁵Pt, and ³¹P NMR spectra were recorded in proton-decoupled mode. Microanalyses were completed by ALS Environmental or Atlantic Microlab. UV–visible absorption spectra were recorded on a Cary 50 or Hewlett-Packard 8452 diode array spectrophotometer in quartz cells. Photolyses were performed in quartz (UV) or borosilicate glass vessels using a Philips PL-S 9W/01 9 W lamp (313 nm emission) or LEDs (superbrightleds.com) of the indicated wavelength.

trans-Pt(PET₃)₂Cl(4-trifluoromethylphenyl) (**2**).



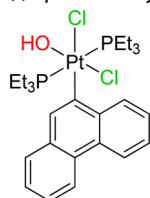
A solution of 1-chloro(4-trifluoromethyl)benzene (23 mg, 0.13 mmol) in THF (~2 mL) was added to a clear orange solution of Pt(PET₃)₄ (70 mg, 0.10 mmol) in THF (~2 mL). The resulting clear orange solution was stirred for ~20 h at 140 °C in a sealed tube to yield a pale yellow solution. The mixture was cooled to ambient temperature, and the volatiles were removed *in vacuo*. The solid residue was dissolved in ~2 mL of CH₂Cl₂ and transferred to a 4 mL vial. The volume was reduced *in vacuo* to ~0.5 mL followed by the addition of ~1 mL of methanol. The vial was capped and stored at -20 °C overnight to afford colorless crystals. The mother liquor was pipetted out, and the crystals were dried *in vacuo* to yield 40 mg (63%) of **2**. ³¹P NMR (101 MHz, CDCl₃): 14.5 (s with satellite, J_{PP} = 2733 Hz). ¹⁹F NMR (235 MHz, CDCl₃): -62.0 (s). ¹H NMR (250 MHz, CDCl₃): 7.47 (d with satellites, J_{HH} = 7.95 Hz, J_{PH} = 65 Hz, 2H), 7.12 (m, 2H), 1.78–1.53 (m, 12H, CH₂), 1.14–1.01 (app quintet, J_{app} = 8.27 Hz, 18H, CH₃).

trans-Pt(PET₃)₂Cl(9-phenanthryl) (**1**). This complex was prepared from 9-chlorophenanthrene by a procedure similar to that for **2**. ³¹P NMR (101 MHz, CD₂Cl₂): 14.10 (s with satellite, J_{PP} = 2735 Hz). ³¹P NMR (101 MHz, C₆D₆): 13.97 (s with satellite, J_{PP} = 2736 Hz). ¹H NMR (250 MHz, CD₂Cl₂): 8.97–8.93 (m, 1H), 8.62–8.57 (m, 2H), 7.82 (s with satellites, J_{PH} = 75 Hz, 1H), 7.69–7.65 (m, 1H), 7.57–7.46 (m, 4H), 1.70–1.40 (m, 12H, CH₂), 1.08–0.96 (app quintet, J = 8.2 Hz, 18H, CH₃). ¹H NMR (250 MHz, C₆D₆): 9.28 (d, J_{HH} = 7.50 Hz, 1H), 8.59 (t, J_{HH} = 7.50 Hz, 2H), 8.09 (s with satellites, J_{PH} = 75.0 Hz, 1H), 7.75 (d, J_{HH} = 7.50 Hz, 1H), 7.58 (t, J_{HH} = 7.50 Hz, 1H), 7.49–7.37 (m, 3H), 1.62–1.28 (m, 12H, CH₂), 0.89–0.77 (app quintet, J = 8.2 Hz, 18H, CH₃).

Preparation of H₂O₂ in Ether.⁶⁰ Approximately 7 mL of 30% H₂O₂ was placed in a 20 mL vial, and then 7 mL of diethyl ether was added. The vial was capped tightly, and the contents were stirred vigorously for a minimum of 2 h. (**Caution!** While we never observed H₂O₂ decomposition and O₂ evolution, this is a possibility and a mechanism for pressure release should be provided.) The ether layer (upper layer) was

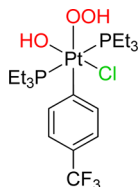
then pipetted into another 20 mL vial. The solution was then concentrated *in vacuo* to 0.5–1 mL. The concentrated solution was not stored but used immediately in the following syntheses.

trans,cis-Pt(PEt₃)₂Cl₂(OH)(9-phenanthryl) (3).



trans-Pt(PEt₃)₂Cl(9-phenanthryl) (1) (10.1 mg, 0.0157 mmol) in 1.5 mL of dichloromethane was mixed in a 20 mL vial with 1 mL of a freshly prepared H₂O₂ solution in diethyl ether. (The preparation of the H₂O₂ solution is described above.) The vial was capped with a rubber septum, and a needle was inserted to release the pressure generated during the reaction. The mixture was stirred and monitored by ³¹P NMR spectroscopy. The colorless solution became yellowish orange, and conversion of 1 (δ 14.1) to product 3 along with small amounts of OPEt₃ (δ 50–60) was observed. (³¹P NMR shifts varied with the water content of the reaction mixture.) An intermediate (5) was detected at δ 6–7 and was gone by the end of the reaction. If the reaction was not complete after 10–12 h, additional H₂O₂ solution was added. Once the reaction was complete, the dichloromethane layer was separated from the aqueous layer (from H₂O₂ decomposition) and washed with 3 × 5 mL of deionized water and then dried over MgSO₄. After filtering, the volatiles were removed *in vacuo*. The resulting solid was redissolved in about 0.5 mL of dichloromethane, and 1 mL of hexane was added. A pale orange precipitate (not identified) formed and was removed by filtration. The yellow filtrate was checked by ³¹P NMR spectroscopy and showed only product 3. The filtrate was concentrated and then stored at –20 °C to obtain 7.4 mg (68%) of yellow 3. Yellow crystals for the X-ray analysis were grown similarly but in an open vial in the freezer. Anal. Calcd (found) for PtP₂Cl₂OC₂₆H₄₀·0.3MeOH·0.5H₂O: C, 44.26 (44.03); H, 5.86 (5.90). (The water and MeOH content was determined by ¹H NMR spectroscopy.) MS (APCI) *m/z*: [M – H]⁺ 695, [(M – H) – HCl]⁺ 659, [(M – H) – HOCl]⁺ 643, [(M – H) – OCH₃]⁺ 608. The fragment isotope patterns matched those predicted. ³¹P NMR (101 MHz, CD₂Cl₂): 3.22 (s with satellites, J_{PtP} = 1740 Hz). ³¹P NMR (101 MHz, C₆D₆): 2.29 (s with satellites, J_{PtP} = 1757 Hz). ¹⁹⁵Pt NMR (64 MHz, CD₂Cl₂): –1754 (t, J_{PtP} = 1751 Hz). ¹H NMR (250 MHz, CD₂Cl₂, CDCl₃): 9.14 (d, J_{HH} = 7.50 Hz, 1H), 8.54 (t, J_{HH} = 7.50 Hz, 2H), 8.18 (s with satellites, J_{PtH} = 50.02 Hz, 1H), 7.78 (d, J_{HH} = 7.50 Hz, 1H), 7.64–7.52 (m, 4H), 2.06–1.99 (m, 12H, CH₂), 1.02–0.89 (app quintet, J_{HH} = 8.0 Hz, 18H, CH₃), –0.13 (s, 1H, OH). The OH group signal was observed only after treating the sample with polymer bound diethylamine and could be eliminated by D₂O addition.

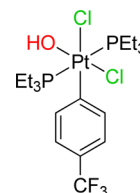
trans-Pt(PEt₃)₂Cl(OH)(OOH)(4-trifluoromethylphenyl) (4).



trans-Pt(PEt₃)₂Cl(4-trifluoromethylphenyl) (2) (13.5 mg, 0.022 mmol) in 1.5 mL of dichloromethane was mixed in a 20 mL vial with a freshly prepared H₂O₂ solution in diethyl ether (1 mL). The vial was capped with a rubber septum, and a needle was inserted to release the pressure generated during the reaction. The mixture was stirred for 3 h at room temperature during which time the solution turned pale yellow and conversion of 2 (δ 14.5) to *trans*-Pt(PEt₃)₂Cl(OH)(OOH)(4-trifluoromethylphenyl) (4) (δ 5–4) was observed by ³¹P NMR spectroscopy (³¹P NMR shifts varied slightly with the water content of the reaction mixture). Once the reaction was complete, the dichloromethane layer was separated, washed with 3 × 5 mL of deionized water and dried with MgSO₄. After filtering, the volatiles were removed *in vacuo*. The resulting

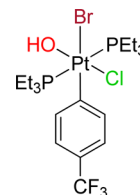
solid was redissolved in about 0.5 mL of dichloromethane, and 1 mL of hexane was added. Evaporation of the solution at –20 °C yielded 13 mg (89%) of pale yellow crystals that were suitable for X-ray analysis. ³¹P NMR (101 MHz, CDCl₃): 1.09 (s with satellite, J_{PtP} = 1770 Hz). ¹⁹F NMR (235 MHz, CDCl₃): –62.27 (s). ¹H NMR (250 MHz, CDCl₃): 8.05 (d with satellites, J_{HH} = 7.50 Hz, J_{PtH} = 45 Hz, 1H), 7.88 (d with satellites, J_{HH} = 7.50 Hz, J_{PtH} = 45 Hz, 1H), 7.29 (m, 2H), 6.42 (s, 1H, OOH), 2.00–1.89 (m, 12H, CH₂), 1.11–1.00 (app quintet, J_{app} = 7.9 Hz, 18H, CH₃), 0.20 (s with satellites, J_{PtH} = 40 Hz, 1H, OH). The OH group signal is concentration dependent in CDCl₃ (and CD₂Cl₂). As concentration increases (above ~0.01 mol L^{–1}), the signal broadens and the ¹⁹⁵Pt satellites move in and eventually merge with the main peak. The OOH signal also broadens. D₂O addition causes complete loss of the OH and OOH signals.

trans,cis-Pt(PEt₃)₂(Cl)₂(OH)(4-trifluoromethylphenyl) (6).



Compound 4 was dissolved in 1 mL of dichloromethane and approximately 2 mL of deionized water, 0.05 mL of dilute HCl (50 μL of conc HCl in 1–2 mL water) was added, and the mixture was stirred for 1 min. ³¹P NMR spectroscopy showed complete conversion of 4 to 6 (δ 1.09). The dichloromethane layer was washed with 10 mL of deionized water and dried with MgSO₄. After filtration, the volatiles were removed *in vacuo*. The resulting solid was washed with 1.0 mL of cold hexane and dried *in vacuo* to give 12.0 mg (88%) of 6. Pale yellow crystals for the X-ray analysis were grown in ether/heptane (1:5) by slow evaporation in the freezer. ³¹P NMR (101 MHz, CDCl₃ or CD₂Cl₂): 1.09 (s with satellites, J_{PtP} = 1708 Hz). ³¹P {¹H} NMR (101 MHz, C₆D₆): 0.16 (s with satellites, J_{PtP} = 1708 Hz). ¹⁹F NMR (235 MHz, CDCl₃ or CD₂Cl₂): –62.30. ¹⁹⁵Pt NMR (64 MHz, CDCl₃): –1944 (t, J_{PtP} = 1720 Hz). ¹H NMR (250 MHz, CDCl₃): 8.16 (d with satellites, J_{HH} = 7.50 Hz, J_{PtH} = 42 Hz, 1H), 7.93 (d with satellites, J_{HH} = 7.50 Hz, J_{PtH} = 42 Hz, 1H), 7.33 (m, 2H), 2.00–1.85 (m, 12H, CH₂), 1.13–1.03 (app quintet, J_{app} = 8.0 Hz, 18H, CH₃), –0.48 (s with satellites, J_{PtH} = 40 Hz, 1H, OH). The OH group signal is concentration dependent in CDCl₃ (and CD₂Cl₂). As concentration increases (above ~0.01 mol L^{–1}), the signal broadens and the ¹⁹⁵Pt satellites move in and eventually merge with the main peak. D₂O addition causes complete loss of the OH signal. ¹H NMR (250 MHz, C₆D₆): 8.41 (d with satellites, J_{HH} = 8.25 Hz, J_{PtH} = 42 Hz, 1H), 8.25 (d with satellites, J_{HH} = 8.25 Hz, J_{PtH} = 38.5 Hz, 1H), 7.36 (d, J_{HH} = 8.25 Hz, 1H), 7.31 (d, J_{HH} = 8.25 Hz, 1H), 1.78–1.63 (m, 12H, CH₂), 0.81–0.68 (app quintet J_{app} = 8.0 Hz, 18H, CH₃), –0.4 (br s, 1H, OH).

trans-Pt(PEt₃)₂(Br)(Cl)(OH)(4-trifluoromethylphenyl) (7).



Compound 4 was dissolved in 1 mL of dichloromethane, approximately 2 mL of deionized water and 0.05 mL of 50% HBr was added, and the mixture was stirred for 1 min. ³¹P NMR spectroscopy showed complete conversion of 4 to 7 (δ –2.09). The dichloromethane layer was washed with 10 mL of deionized water and dried with MgSO₄. After filtering, the volatiles were removed *in vacuo*. The resulting solid was washed with 1.0 mL of cold hexane and dried *in vacuo* to give 7. Pale yellow crystals for the X-ray analysis were grown in CH₂Cl₂/heptane (1:2) by slow evaporation in the refrigerator. ³¹P {¹H} NMR (101 MHz, CD₂Cl₂): –2.09 (s with satellite, J_{PtP} = 1703 Hz). ¹H NMR (250 MHz, CD₂Cl₂): 8.15 (d with

satellites, $J_{\text{HH}} = 7.50$ Hz, $J_{\text{PH}} = 44$ Hz, 1H), 7.95 (d with satellites, $J_{\text{HH}} = 9.50$ Hz, $J_{\text{PH}} = 39$ Hz, 1H), 7.38–7.34 (m, 2H), 2.00–1.86 (m, 12H, CH₂), 1.11–0.98 (app quintet, $J_{\text{app}} = 7.75$ Hz, 18H, CH₃), –0.6 (brs, 1H, OH).

UV–Visible Absorption Spectra. *trans,cis*-Pt(PEt₃)₂(OH)Cl₂(9-phenanthryl) (**3**) (3.2 mg, 0.0046 mmol) was dissolved in HPLC grade CH₂Cl₂ and diluted to the mark in a 5.00 mL volumetric flask. This solution (0.92 mM) was used as a stock solution for the analysis. A series of concentrations was prepared by diluting 40, 50, 60, 70, and 80 μL into 5.0 mL volumetric flasks. The solvent blank was obtained, and spectra were recorded from 200 to 800 nm for each sample. *trans*-Pt(PEt₃)₂(OH)Cl₂(4-trifluoromethylphenyl) (**6**) (20.1 mg, 0.0303 mmol) was dissolved in HPLC grade CH₂Cl₂ and diluted to the mark in a 10.00 mL volumetric flask. This stock solution (3.03 mM) was used to prepare a series of concentrations by diluting 20, 30, 40, and 50 μL into 5.0 mL volumetric flasks. All the experimental conditions were kept identical for **3** and **6** except for the concentrations. The absorbance data collected for the above samples were converted to molar extinction coefficient, averaged, and plotted (Figure 4).

Preparation of HOCl from Ca(OCl)₂. Solid Ca(OCl)₂ (100 mg, 0.70 mmol) was added to a 100 mL Schlenk flask. The stopcock plug was removed from the flask and replaced with a rubber septum. The flask was then connected to a vacuum line. Solvent (H₂O, C₆D₆, or CDCl₃; 0.50 mL) was added into a 5 mm NMR tube. The tube was connected to the vacuum line and immersed in LN₂. The frozen NMR tube and the Schlenk flask were connected and kept under vacuum for 10 min. After reaching a vacuum of 50 mTorr, the connection to the vacuum line was closed and concentrated H₂SO₄ or HCl (0.10 mL) was injected through the rubber septum onto the solid Ca(OCl)₂. (The Schlenk flask was isolated from the NMR tube prior to the addition of H₂SO₄ and reconnected 5 min postinjection.) The gaseous products were condensed into the NMR tube. The tube was thawed, and the solution was transferred into a 1 cm path length quartz cuvette for recording of the UV–vis absorption spectrum (Figure S2, Supporting Information). Solid NaOH (~20 mg, 0.50 mmol) was added to the cuvette with stirring. The spectrum was recorded and showed λ_{max} for the ClO[–] at 292 nm, as reported in previous studies.⁶¹

Synthesis of HOCl from HgO and Cl₂.²⁰ Freshly prepared HgO (100 mg, 0.46 mmol) was added to 2 mL of double distilled water (DDW) in an 8 mL vial. Chlorine gas (1 mL, 0.045 mmol), dissolved in 1 mL of DDW, was immediately added, and the mixture was stirred for 30 min. Filtration through diatomaceous earth yielded a clear solution. The solution was transferred to a 1 cm path length cuvette, and the UV–vis absorption spectrum was recorded (Figure S2, Supporting Information).

Reaction of HOCl with TME. (A) HOCl was generated from Ca(OCl)₂ as described above, but the gaseous products were condensed into a mixture of CDCl₃ (0.50 mL) and TME (2,3-dimethyl-2-butene, ~30 μL) instead of water. The mixture was thawed, and ¹H NMR analysis indicated the formation of TME products (Chart 1). (B) A solution of HOCl from HgO and Cl₂ was generated as described above but with water-saturated CDCl₃ as the solvent instead of DDW. After the NMR tube was thawed, TME was added, and the mixture was analyzed by ¹H NMR spectroscopy.

Photolysis of HOCl. Three identical samples of HOCl in C₆D₆ were prepared from Ca(OCl)₂ as described above. TME (~30 μL) was added to one, and the products were determined by ¹H NMR spectroscopy (Chart 1). Another sample was photolyzed at 313 nm for 8 min, and then TME was added. No TME products were observed except for **11** (TME and Cl₂ yields **11**). The third sample was photolyzed at 380 nm for 8 min, and then TME was added. No TME oxidation was detected. In other experiments, C₆H₆ samples of HOCl were photolyzed at 313 and 380 nm without trap. Chlorobenzene was detected by ¹H NMR in both samples.

Reaction of HOCl with PPh₃ and **1.** PPh₃ (3.5 mg, 0.015 mmol) was dissolved in 0.8 mL of C₆D₆. A dilute C₆D₆ solution of HOCl, prepared by diluting a 0.05 mL aliquot of a C₆D₆ HOCl solution (prepared from Ca(OCl)₂ as described above) to 0.4 mL, was added in

portions until the ³¹P NMR signal for PPh₃ (δ –4.9) disappeared. The only product detected by ³¹P NMR spectroscopy was OPh₃ (δ 28.0).

Reaction of HOCl with **1 or **2**.** A solution of **1** (0.02 M) in C₆D₆ was mixed with a 0.05 mL aliquot of HOCl made in C₆D₆ (prepared from Ca(OCl)₂). The ³¹P NMR signal for **8** was observed. The only product detected by ³¹P NMR spectroscopy was **8** and remaining **1**. A similar experiment was carried out with **2** and yielded **9**.

Reaction of photolyzed **3 with PPh₃.** A sample of **3** (2.0 mg, 0.0029 mmol) was photolyzed at 313 nm in ~0.5 mL of C₆D₆ until all **3** had been consumed. Excess PPh₃ (5 mg, 0.019 mmol) was added. A 22% yield of OPh₃ was observed by ³¹P NMR spectroscopy.

Photolysis of *trans,cis*-Pt(PEt₃)₂Cl₂(OH)(9-phenanthryl) (3**).** Photolysis experiments were performed at 313 and 380 nm in C₆D₆ and CD₂Cl₂. A 0.011 M solution of **3** was added to a 5 mm J. Young NMR tube. Photolysis was then carried out with periodic ³¹P NMR and ¹H NMR monitoring. Compound **3** was observed to convert to **1** (colorless) although the solution remained yellow orange and did not become colorless as expected for **1**.

Photolysis of *trans,cis*-Pt(PEt₃)₂Cl₂(OH)(4-trifluoromethylphenyl) (6**).** The photolysis experiments were performed at 313 nm in CDCl₃, CD₂Cl₂, and C₆D₆. Solutions of **6** (0.018 M) were photolyzed in the presence of variable amounts of TME. Irradiation times were 14–17 min. Spectroscopic analysis (NMR) was carried out within 5 min of the photolysis, and the results are given in Table 4.

Photolysis of **6 in the Presence of **2**.** A 5 mm NMR tube was charged with 0.5 mL of a CH₂Cl₂ solution that was 0.018 M in **6** and 0.016 M in **2**. A capillary tube containing a solution of PPh₃ was added to the tube to serve as an integration standard. The sample was then photolyzed at 313 nm. ³¹P NMR analysis was carried out at 30 s intervals until all **6** was consumed (13 min total). At the end of the photolysis, a 48% conversion of **2** into trichloro complex **9** was indicated. A maximum conversion of 50% is expected from the available chlorine in **6**.

Photolysis of *trans*-Pt(PEt₃)₂(Br)(Cl)(OH)(4-trifluoromethylphenyl) (7**).** The photolysis experiments were performed similarly to those for **6** in CD₂Cl₂ both with and without TME. The bromohydrin **16** was identified by comparison of the NMR properties (¹H NMR in CDCl₃; δ 1.84, 1.35) with an authentic sample prepared by HBr addition to the epoxide. NMR data for **17** have been reported.⁶²

NMR Data for *trans*-Pt(PEt₃)₂(Br)(4-trifluoromethylphenyl) (15**).** ³¹P {¹H} NMR (101 MHz, CD₂Cl₂): 12.4 (s with satellite, $J_{\text{PP}} = 2709$ Hz). ¹H NMR (250 MHz, CD₂Cl₂): 7.50 (d with satellites, $J_{\text{HH}} = 10$ Hz, $J_{\text{PH}} = 67.50$ Hz, 2H), 7.17–7.11 (m, 2H), 1.74–1.59 (m, 12H, CH₂), 1.12–0.99 (app quintet, $J_{\text{app}} = 8.10$ Hz, 18H, CH₃).

Quantum Yield Determinations. Irradiations were performed in the compartment of a Cary 50 UV–vis spectrometer equipped with a magnet stirrer and temperature control. The sample was contained in a 1 cm quartz cuvette sealed at the top with a quartz microscope slide. The light source was positioned over the sample compartment, allowing irradiations through the top of the cuvette.⁶³ The photon flux was measured (Fe oxalate actinometry^{64,65}) before and after each sample irradiation, and the average of the before and after measurements was used as the photon flux during the sample irradiation. Sample solution concentrations were sufficiently high to ensure complete photon absorption (absorbance ≥ 2 at the irradiation wavelength) over the ~3 cm depth of the solution. Reaction progress was monitored by the UV–vis absorbance of product *trans*-Pt(PEt₃)₂Cl₃(4-trifluoromethylphenyl) (**8**) over the region of 310–400 nm where *trans*-Pt(PEt₃)₂Cl₂(4-trifluoromethylphenyl) (**2**) does not absorb and *trans*-Pt(PEt₃)₂Cl₂(OH)(4-trifluoromethylphenyl) (**6**) absorbance is relatively weak. The yield of **8** from the UV–vis (0.3 mM) data is 34% and matches the yield determined by ³¹P NMR spectroscopy (1 mM). The absorbance increase at three wavelengths (365, 375, and 390 nm) during the first 10% of the reaction was used to calculate the quantum yield. The average of three runs gave a final quantum yield for **6** of 51% \pm 2% in dichloromethane.

Computational Details. Gaussian 09 (revision A.1 or C.1)⁶⁶ with the M06⁶⁷ or CAM-B3LYP⁶⁸ (TDDFT) functional was used for all calculations. The LANL2DZ^{69–72} basis set was employed for Pt, Cl,

and P with an added d function ($\alpha = 0.05$) for Pt, d ($\alpha = 0.648$) and p ($\alpha = 0.0467$) functions for Cl, and d ($\alpha = 0.434$) and p ($\alpha = 0.0376$) functions for P.⁷³ The 6-31G(d) basis set was used for all other atoms. Initial structures were derived from crystal coordinates and were modified with Gaussview.^{74,75} All geometries were optimized with no symmetry constraints in the gas phase. Free energies, enthalpies, and entropies were calculated at 298.15 K and 1 atm. Analytical frequency calculations gave no imaginary frequencies for the complexes except for 3', which had a small imaginary frequency of -11 cm^{-1} associated with a methyl group rotation. Coordinates and energies are given in Tables S1–S19, Supporting Information. TDDFT and other indicated calculations included solvent (dichloromethane) with the polarized continuum model (pcm)⁷⁶ and employed the gas-phase optimized structures.

■ ASSOCIATED CONTENT

● Supporting Information

CIF files, additional experimental details, NMR spectra, and DFT data (coordinates, energies, NTO figures). This material is available free of charge via the Internet at <http://pubs.acs.org>.

■ AUTHOR INFORMATION

Corresponding Author

*Paul R. Sharp. E-mail: sharp@missouri.edu.

Author Contributions

The manuscript was written through contributions of all authors. All authors have given approval to the final version of the manuscript.

Notes

The authors declare no competing financial interest.

■ ACKNOWLEDGMENTS

Support was provided by the U.S. Department of Energy, Office of Basic Energy Sciences (Grant DE-FG02-88ER13880). We thank Dr. Charles Barns for X-ray data collection and processing, Tharushi Perera for the synthesis of 1, Dr. Wei Wycoff for assistance with the NMR measurements, and Dr. Nathan Lee for mass spectral analyses. The computations were performed on the HPC resources at the University of Missouri Bioinformatics Consortium (UMBC).

■ REFERENCES

- (1) Esswein, A. J.; Nocera, D. G. *Chem. Rev.* **2007**, *107*, 4022–4047.
- (2) Nocera, D. G. *Inorg. Chem.* **2009**, *48*, 10001–10017.
- (3) Cook, T. R.; Surendranath, Y.; Nocera, D. G. *J. Am. Chem. Soc.* **2009**, *131*, 28–29.
- (4) Teets, T. S.; Nocera, D. G. *J. Am. Chem. Soc.* **2009**, *131*, 7411–7420.
- (5) Kohl, S. W.; Weiner, L.; Schwartsburd, L.; Konstantinovski, L.; Shimon, L. J. W.; Ben-David, Y.; Iron, M. A.; Milstein, D. *Science* **2009**, *324*, 74–77.
- (6) Chen, Y.; Fang, W.-H. *J. Phys. Chem. A* **2010**, *114*, 10334–10338.
- (7) Petruzzella, E.; Margiotta, N.; Ravera, M.; Natile, G. *Inorg. Chem.* **2013**, *52*, 2393–2403.
- (8) Vogler, A.; Kunkely, H. *Inorg. Chem. Commun.* **2011**, *14*, 96–98.
- (9) Becht, A.; Vogler, A. *Inorg. Chem.* **1993**, *32*, 2835–2837.
- (10) Knor, G.; Vogler, A.; Roffia, S.; Paolucci, F.; Balzani, V. *Chem. Commun.* **1996**, 1643–1644.
- (11) Karikachery, A. R.; Lee, H. B.; Masjedi, M.; Ross, A.; Moody, M. A.; Cai, X.; Chui, M.; Hoff, C.; Sharp, P. R. *Inorg. Chem.* **2013**, *52*, 4113–4119.
- (12) Wick, D. D.; Goldberg, K. I. *J. Am. Chem. Soc.* **1999**, *121*, 11900–11901.
- (13) Rostovtsev, V. V.; Henling, L. M.; Labinger, J. A.; Bercaw, J. E. *Inorg. Chem.* **2002**, *41*, 3608–3619.
- (14) Allen, F. H. *Acta Crystallogr.* **2002**, *B58*, 380–388.
- (15) Smythe, N. A.; Grice, K. A.; Williams, B. S.; Goldberg, K. I. *Organometallics* **2008**, *28*, 277–288.
- (16) Poverenov, E.; Efremenko, I.; Frenkel, A. I.; Ben-David, Y.; Shimon, L. J. W.; Leitun, G.; Konstantinovski, L.; Martin, J. M. L.; Milstein, D. *Nature* **2008**, *455*, 1093–1096.
- (17) Martin, R. L. *J. Chem. Phys.* **2003**, *118*, 4775–4777.
- (18) Unangst, P. C. *e-EROS Encyclopedia of Reagents for Organic Synthesis*; John Wiley & Sons, Ltd: New York, 2001.
- (19) Wojtowicz, J. A. *Kirk-Othmer Encyclopedia of Chemical Technology*; John Wiley & Sons, Inc.: New York, 2000.
- (20) Cady, G. H. *Inorg. Synth.* **1957**, *5*, 156–165.
- (21) Vogt, R.; Schindler, R. N. *J. Photochem. Photobiol., A: Chem.* **1992**, *66*, 133–140.
- (22) Oxley, J. C.; Smith, J. L.; Chen, H. *Propellants, Explos., Pyrotech.* **2002**, *27*, 209–216.
- (23) Foote, C. S.; Wexler, S.; Ando, W.; Higgins, R. J. *Am. Chem. Soc.* **1968**, *90*, 975–981.
- (24) DeRosa, M. C.; Crutchley, R. J. *Coord. Chem. Rev.* **2002**, 233–234, 351–371.
- (25) Luo, Y.-R. *Comprehensive Handbook of Chemical Bond Energies*; CRC Press: Boca Raton, FL, USA, 2007.
- (26) Ford, P. C. *Coord. Chem. Rev.* **1982**, *44*, 61–82.
- (27) Ford, P. C.; Wink, D.; Dibenedetto, J. In *Progress Inorganic Chemistry*; Lippard, S. J., Ed.; John Wiley & Sons, Inc.: New York, 1983, pp 213–271.
- (28) Langford, C. H.; Malkhasian, A. Y. S. *J. Am. Chem. Soc.* **1987**, *109*, 2682–2685.
- (29) Goursot, A.; Kirk, A. D.; Waltz, W. L.; Porter, G. B.; Sharma, D. K. *Inorg. Chem.* **2002**, *26*, 14–18.
- (30) Salassa, L.; Garino, C.; Salassa, G.; Gobetto, R.; Nervi, C. *J. Am. Chem. Soc.* **2008**, *130*, 9590–9597.
- (31) Zheldakov, I. L.; N. Ryazantsev, M.; Tarnovsky, A. N. *J. Phys. Chem. Lett.* **2011**, *2*, 1540–1545.
- (32) Glebov, E. M.; Kolomeets, A. V.; Pozdnyakov, I. P.; Plyusnin, V. F.; Grivin, V. P.; Tkachenko, N. V.; Lemmetyinen, H. *RSC Adv.* **2012**, *2*, 5768–5778.
- (33) Babaeva, A. V. *Dokl. Akad. Nauk SSSR* **1939**, *23*, 653.
- (34) Kuroda, R.; Neidle, S.; Ismail, I. M.; Sadler, P. J. *Inorg. Chem.* **1983**, *22*, 3620–3624.
- (35) Brandon, R. J.; Dabrowiak, J. C. *J. Med. Chem.* **1984**, *27*, 861–865.
- (36) Vollano, J. F.; Blatter, E. E.; Dabrowiak, J. C. *J. Am. Chem. Soc.* **1984**, *106*, 2732–2733.
- (37) Al-Baker, S.; Dabrowiak, J. C. *Inorg. Chem.* **1987**, *26*, 613–617.
- (38) Thorshaug, K.; Fjeldahl, I.; Romming, C.; Tilset, M. *Dalton Trans.* **2003**, 4051–4056.
- (39) Murray, P.; Koch, K. R. *J. Coord. Chem.* **2010**, *63*, 2561–2577.
- (40) Rashidi, M.; Nabavizadeh, M.; Hakimelahi, R.; Jamali, S. J. *Chem. Soc., Dalton Trans.* **2001**, 3430–3434.
- (41) Pellarin, K. R.; McCready, M. S.; Sutherland, T. I.; Puddephatt, R. J. *Organometallics* **2012**, *31*, 8291–8300.
- (42) Nakabayashi, Y.; Erxleben, A.; Létinois, U.; Pratviel, G.; Meunier, B.; Holland, L.; Lippert, B. *Chem.—Eur. J.* **2007**, *13*, 3980–3988.
- (43) Glebov, E. M.; Plyusnin, V. F.; Grivin, V. P.; Venediktov, A. B.; Korenev, S. V. *Russ. Chem. Bull.* **2007**, *56*, 2357–2363.
- (44) Balzani, V.; Manfrin, M. F.; Moggi, L. *Inorg. Chem.* **1967**, *6*, 354–358.
- (45) Penkett, S. A.; Adamson, A. W. *J. Am. Chem. Soc.* **1965**, *87*, 2514–2515.
- (46) Grice, K. A.; Scheuermann, M. L.; Goldberg, K. I. *Top. Organomet. Chem.* **2011**, *35*, 1–27.
- (47) Labinger, J. A.; Herring, A. M.; Lyon, D. K.; Luinstra, G. A.; Bercaw, J. E.; Horvath, I. T.; Eller, K. *Organometallics* **1993**, *12*, 895–905.
- (48) Labinger, J. A.; Herring, A. M.; Bercaw, J. E. *J. Am. Chem. Soc.* **1990**, *112*, 5628–5629.
- (49) DeVries, N.; Roe, D. C.; Thorn, D. L. *J. Mol. Catal. A: Chem.* **2002**, *189*, 17–22.

- (50) Oblad, P. F.; Bercaw, J. E.; Hazari, N.; Labinger, J. A. *Organometallics* **2010**, *29*, 789–794.
- (51) Shibaeva, R. P.; Rozenberg, L. P.; Lobkovskaya, R. M.; Shilov, A. E.; Shul'pin, G. B. *J. Organomet. Chem.* **1981**, *220*, 271–276.
- (52) Glebov, E. M.; Grivin, V. P.; Plyusnin, V. F.; Venediktov, A. B.; Korenev, S. V. *J. Photochem. Photobiol., A* **2010**, *214*, 181–187.
- (53) Glebov, E. M.; Plyusnin, V. F.; Venediktov, A. B.; Korenev, S. V. *Russ. Chem. Bull.* **2003**, *52*, 1305–1311.
- (54) Fadnis, A. G.; Kemp, T. J. *J. Chem. Soc., Dalton Trans.* **1989**, 1237–1240.
- (55) Waltz, W. L.; Lilie, J.; Goursot, A.; Chermette, H. *Inorg. Chem.* **1989**, *28*, 2247–2256.
- (56) Rehorek, D.; Dubose, C. M.; Janzen, E. G. *Inorg. Chim. Acta* **1984**, *83*, L7–L8.
- (57) Wright, R. C.; Laurence, G. S. *J. Chem. Soc., Chem. Commun.* **1972**, 132–133.
- (58) van Slageren, J.; Klein, A.; Zálaiš, S. *Coord. Chem. Rev.* **2002**, *230*, 193–211.
- (59) Yoshida, T.; Matsuda, T.; Otsuka, S. *Inorg. Synth.* **1990**, *28*, 119–121.
- (60) Saito, I.; Nagata, R.; Yuba, K.; Matsuura, T. *Tetrahedron Lett.* **1983**, *24*, 1737–1740.
- (61) Feng, Y.; Smith, D. W.; Bolton, J. R. *J. Environ. Eng. Sci.* **2007**, *6*, 277–284.
- (62) Clennan, E. L.; Chen, X. *J. Am. Chem. Soc.* **1989**, *111*, 5787–5792.
- (63) Comerford, J. J. *Varian Instrum. Work* **2003**, *87*, 1–8.
- (64) Hatchard, C. G.; Parker, C. A. *Proc. R. Soc. London, Ser. A* **1956**, *235*, 518–536.
- (65) Kurien, K. C. *J. Chem. Soc. B* **1971**, 2081–2082.
- (66) Frisch, M. J.; Trucks, G. W.; Schlegel, H. B.; Scuseria, G. E.; Robb, M. A.; Cheeseman, J. R.; Scalmani, G.; Barone, V.; Mennucci, B.; Petersson, G. A.; Nakatsuji, H.; Caricato, M.; Li, X.; Hratchian, H. P.; Izmaylov, A. F.; Bloino, J.; Zheng, G.; Sonnenberg, J. L.; Hada, M.; Ehara, M.; Toyota, K.; Fukuda, R.; Hasegawa, J.; Ishida, M.; Nakajima, T.; Honda, Y.; Kitao, O.; Nakai, H.; Vreven, T.; Montgomery, J. A., Jr.; Peralta, J. E.; Ogliaro, F.; Bearpark, M.; Heyd, J. J.; Brothers, E.; Kudin, K. N.; Staroverov, V. N.; Kobayashi, R.; Normand, J.; Raghavachari, K.; Rendell, A.; Burant, J. C.; Iyengar, S. S.; Tomasi, J.; Cossi, M.; Rega, N.; Millam, J. M.; Klene, M.; Knox, J. E.; Cross, J. B.; Bakken, V.; Adamo, C.; Jaramillo, J.; Gomperts, R.; Stratmann, R. E.; Yazyev, O.; Austin, A. J.; Cammi, R.; Pomelli, C.; Ochterski, J. W.; Martin, R. L.; Morokuma, K.; Zakrzewski, V. G.; Voth, G. A.; Salvador, P.; Dannenberg, J. J.; Dapprich, S.; Daniels, A. D.; Farkas, O.; Foresman, J. B.; Ortiz, J. V.; Cioslowski, J.; Fox, D. J. *Gaussian 09*, revision B.01 or C.01; Gaussian, Inc.: Wallingford, CT, 2009.
- (67) Zhao, Y.; Truhlar, D. G. *Acc. Chem. Res.* **2008**, *41*, 157–167.
- (68) Yanai, T.; Tew, D.; Handy, N. *Chem. Phys. Lett.* **2004**, *393*, 51–57.
- (69) Dunning, T. H.; Hay, P. J. *Modern Theoretical Chemistry*; Plenum: New York, 1976; Vol. 3.
- (70) Hay, P. J.; Wadt, W. R. *J. Chem. Phys.* **1985**, *82*, 299.
- (71) Wadt, W. R.; Hay, P. J. *J. Chem. Phys.* **1985**, *82*, 284.
- (72) Hay, P. J.; Wadt, W. R. *J. Chem. Phys.* **1985**, *82*, 270.
- (73) Check, C. E.; Faust, T. O.; Bailey, J. M.; Wright, B. J.; Gilbert, T. M.; Sunderlin, L. S. *J. Phys. Chem. A* **2001**, *105*, 8111.
- (74) Dennington, R.; Keith, T.; Millam, J. *GaussView*, version 5.0.8; Semichem Inc.: Shawnee Mission, KS, 2009.
- (75) O'Boyle, N. M.; Tenderholt, A. L.; Langner, K. M. *J. Comput. Chem.* **2008**, *29*, 839–845.
- (76) Tomasi, J.; Mennucci, B.; Cammi, R. *Chem. Rev.* **2005**, *105*, 2999–3094.